THE JOURNAL OF PHYSICAL CHEMISTRY B

Article

pubs.acs.org/JPCB

Reactions of Deprotonated Tyrosine and Tryptophan with Electronically Excited Singlet Molecular Oxygen ($a^1\Delta_g$): A Guided-Ion-Beam Scattering, Statistical Modeling, and Trajectory Study

Fangwei Liu, Yigang Fang, Yun Chen, and Jianbo Liu*

Department of Chemistry and Biochemistry, Queens College and the Graduate Center of the City University of New York, 65-30 Kissena Blvd., Flushing, New York 11367, United States

ABSTRACT: The reactions of deprotonated tyrosine ([Tyr-H]$^-$) and tryptophan ([Trp-H]$^-$) with the lowest electronically excited state of molecular oxygen $O_2[a^1\Delta_g]$ have been studied in the gas phase, including the measurement of the effects of collision energy (E_{col}) on reaction cross sections over a center-of-mass E_{col} range from 0.05 to 1.0 eV. [Tyr-H]$^-$ and [Trp-H]$^-$ were generated using electrospray ionization, and both have a pure carboxylate anion structure in the gas phase. Density functional theory calculations and RRKM modeling were used to examine properties of various complexes, transition states, and products that might be important along the reaction coordinate. It was found that deprotonation of Tyr and Trp results in a large effect on their $^1O_2$-mediated oxidation. For [Tyr-H]$^-$, the reaction corresponds to the formation of a hydroperoxide intermediate, followed by intramolecular H transfer and subsequent dissociation to product ion 4-(2-aminovinyl)phenolate, and neutral H_2O_2 and CO_2. Despite that the reaction is 1.83 eV exothermic, the reaction cross section shows a threshold-like behavior at low E_{col} and increases with increasing E_{col}, suggesting that the reaction bears an activation barrier above the reactants. Quasi-classical, direct dynamics trajectory simulations were carried out for [Tyr-H]$^-$ + $^1O_2$ at E_{col} = 0.75 eV, using B3LYP/4−31G* level of theory. Trajectories demonstrated the intermediacy of complexes at the early stage of the reaction. A similar product channel was observed in the reaction of [Trp-H]$^-$ with $^1O_2$, yielding product ion 3-(2-aminovinyl)indol-1-ide, H_2O_2 and CO_2. However, the reaction cross section of [Trp-H]$^-$ is strongly suppressed by E_{col} and becoming negligible at E_{col} > 1.0 eV, indicating that this reaction proceeds without energy barriers above the reactants.

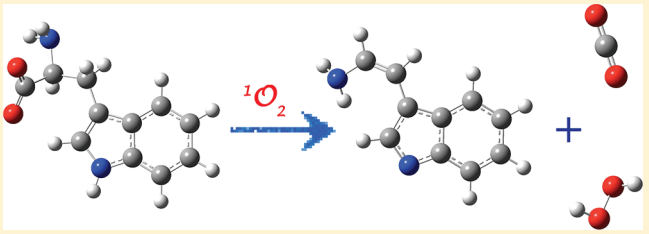

I. INTRODUCTION

Molecular oxygen possesses a unique electronic configuration with the first excited singlet state ($O_2[a^1\Delta_g]$) lying above its triplet ground state ($O_2[X^3\Sigma_g]$).[1] $^1O_2$ has a characteristic chemistry in which molecules are oxygenated,[2−7] setting it apart from $^3O_2$ which, because of two unpaired parallel-spin electrons, does not react with most molecules unless activated by additional energy. $^1O_2$ can be generated in biological systems by energy transfer to $^3O_2$ from protein-bound or other excited chromophores and by enzymatic and nonenzymatic reactions.[8] Consequently, $^1O_2$-mediated oxygenation reactions are involved in the progression of cell death, biological aging, and diseases[8−10] and in photodynamic therapy where $^1O_2$ is used to kill cancer cells.[11] Proteins are the most significant intracellular target for $^1O_2$-mediated oxidative damage,[12] and tyrosine (Tyr) and tryptophan (Trp) are among the residues that are most susceptible to such damage because of their electron-rich side chains being favored by $^1O_2$.[8,10,13]

Most experiments devoted to the elucidation of the $^1O_2$-mediated oxidation mechanisms of amino acids were carried out in solution using photosensitization methods[14] (referred to as "photooxidation"), where $^1O_2$ was generated with ultraviolet or visible light in the presence of sensitizers (i.e., sensitizer $\xrightarrow{h\nu}$ sensitizer*, followed by sensitizer* + $^3O_2 \xrightarrow{\text{energy transfer}}$ sensitizer + $^1O_2$).[15] $^1O_2$-mediated photooxidation of free, zwitterionic Tyr has been proposed to proceed via a ring closure process to form an endoperoxide that undergoes rapid ring-opening to give a hydroperoxide, which subsequently dissociates into a corresponding alcohol.[16,17] It was found that CO_2 was produced during photooxidation of Tyr.[16,18] One important feature observed in solution-phase photooxidation of Tyr is its sharp pH dependence with an inflection point at pH 10.1.[5,19−29] At pH lower than 8.5, the phenolic −OH group is un-ionized, and physical quenching of $^1O_2$ by Tyr largely prevails with regeneration of $^3O_2$. Direct chemical reactions account for at most a few percent of total quenching,[26,30] and the reaction rate constant is lower compared to other amino acids.[31] At the pH range of 11 to 12, ionization of the phenolic proton (note that the pI value of Tyr is 5.7, while the pK_a value of its phenolic ring is 10.1[32]) favors the reaction of the resulting phenoxide anion with $^1O_2$, with the overall rate constant increases by 2 orders of magnitude relative to nonionized Tyr.[24,28] This

Received: March 29, 2012
Revised: May 8, 2012
Published: May 14, 2012

confirms that the ionized phenolic group dominates the reaction with $^1O_2$ in solution, possibly because the enhanced electron releasing ability of the phenoxide anion prompts a charge transfer route leading to oxidation products.[28] Note that in aqueous solution the most acidic site in Tyr is the carboxyl group, and the conjugate base is a carboxylate anion at physiological pH. As a result, the carboxylate anion of Tyr may be considered as a more suitable substrate in biological systems than the phenoxide anion. However, photooxidation of the carboxylate anion by $^1O_2$ has not been well addressed, and oxidation products remain unidentified.[8,13,16,17]

$^1O_2$-mediated photooxidation of Trp is also complex, involving multiple steps and intermediates.[33−38] Reaction initially yields a dioxetane intermediate **1** across the C2−C3 double bond on the indole side chain; alternatively, the reaction can form an energetically more favorable intermediate 3-hydroperoxy-indolenine **2**. Subsequent C2−C3 bond cleavage of **1** yields *N*-formylkynurenine **3**. **2** undergoes an intramolecular addition to form 3α-hydroperoxyhexahydropyrroloindole **4**, followed by rearrangement to **3** or reduction to 3α-hydroxyhexahydropyrroloindole **5**. Decomposition of **5** also results in **3**. Recently, H_2O_2 was detected on Trp hydroperoxide decomposition.[37] A scheme summarizing these reaction paths was present in our paper of protonated Trp oxidation.[39] In addition to chemical reactions, Trp gives rise to significant physical quenching of $^1O_2$.[31,40] $^1O_2$-meditaed photooxidation of Trp also shows a strong dependence on pH,[20,33] and a maximum reactivity was observed between pH 8.0 and 8.5. The origin of this pH dependence seems not completely due to ionization of Trp carboxylic acid or ammonium group, as glycyl-Trp and *N*-acetyl-Trp exhibited a similar pH dependence.[20] Neither is this due to the ionization of the indole ring, since the pK_a value of the indole ring is much higher (i.e., 16.82).[41] Most likely, the pH dependence is due to the formation and breakdown of different intermediate complexes. pH dependence has also been observed in photooxidation of histidine,[20,21,23,29,31] methionine,[4,20,22,42] and cysteine.[4,5,23] Such pH dependence explains the wide variation in literature values of $^1O_2$ reaction rate constants with various amino acids. Likewise, the ability of $^1O_2$ to react with and to damage particular residues in biological systems will depend on the pH at cellular locations.[29]

Recently, we reported the reactions of protonated tyrosine ($TyrH^+$)[43] and tryptophan ($TrpH^+$)[39] with $^1O_2$ in the gas phase, using electrospray-ionization (ESI)[44,45] and guided-ion-beam scattering methods.[46] Gas-phase study avoids the complexities associated with photooxidation experiments (e.g., pH, oxygen concentration, solvent composition and polarity, combination of light and sensitizer, competition between radical- and $^1O_2$-mediated reactions).[7] By combining the input of gas-phase experiments and theoretical approaches, we were able to unravel reaction dynamics for $TyrH^+ + {}^1O_2$ and $TrpH^+ + {}^1O_2$ in depth and established elaborate reaction mechanisms. Gas-phase reaction of $TyrH^+$ with $^1O_2$ leads to generation of H_2O_2 via transfer of two H atoms from $TyrH^+$ to O_2, while the reaction of $TrpH^+$ results in dissociation of a $TrpOOH^+$ intermediate into a glycine molecule and charged indole side chain in addition to ground-state O_2. These results have prompted us to carry out a study on the gas-phase reactions of deprotonated tyrosine ($[Tyr-H]^-$) and tryptophan ($[Trp-H]^-$)[39] with $^1O_2$, aimed at helping attain a better understanding of the pH dependence of Tyr and Trp oxidation. We measured the reaction cross sections of $[Tyr-H]^- + {}^1O_2$ and $[Trp-H]^- + {}^1O_2$ over a wide range of collision energies (E_{col}). E_{col} dependence of the reaction cross sections gives information about interchannel competition and the effects of energy. To supplement gas-phase experiments and unravel reaction mechanisms, electronic structure calculations and Rice−Ramsperager−Kassel−Marcus (RRKM) theory[47] were used to find complexes, transitions states and products along the reaction coordinate, and predict their properties. Finally, direct dynamics simulations[48] were used to provide additional mechanistic insights. Compared to the study of $^1O_2$ reactions in solution, much less is known about ion-chemistry with $^1O_2$ in the gas-phase.[43,49−62] The handful of recent ion−molecule reaction studies involving $^1O_2$ were mostly on the reactions of small negative ions which are more relevant to ionospheric chemistry.[56−62] To the best of our knowledge, the present study represents a first detailed report on gas-phase negative biomolecular ion-electronically excited molecule reaction dynamics. The study serves to demonstrate the importance of ionizable protons in gas-phase $^1O_2$-mediated oxidation of Tyr and Trp, establishing the dependence of oxidation mechanisms on protonation/deprotonation of amino acid moieties.

The remainder of the paper is organized as follows. Section II describes the guided-ion-beam scattering methods used to measure the gas-phase reactions of $[Tyr-H]^-$ and $[Trp-H]^-$ with $^1O_2$ and the density functional theory (DFT) calculations, RRKM modeling, and quasi-classical direct dynamics trajectory simulations used to investigate reaction dynamics. Reaction results are presented in section III, starting with product ions and cross sections of $[Tyr-H]^-$ and $[Trp-H]^-$ with $^1O_2$, and comparison with the results of $TyrH^+$ and $TrpH^+$, proceeding to the construction of the reaction coordinate for $[Tyr-H]^- + {}^1O_2$ and $[Trp-H]^- + {}^1O_2$ using DFT calculations, and finally to the analysis of dynamics trajectory results of $[Tyr-H]^- + {}^1O_2$ and statistical modeling of $[Trp-H]^- + {}^1O_2$. Conclusions are presented in section IV.

II. EXPERIMENTAL AND COMPUTATIONAL DETAILS

A. Experimental Procedures. All experiments were carried out on a home-built guided-ion-beam tandem mass spectrometer that couples with an ESI source. Details of the instrument have been provided in previous papers,[39,43,49,63,64] except that in the present study the apparatus was operated in the negative ion mode. The apparatus consists of an ion source, radio frequency (rf) hexapole ion guide, quadrupole mass filter, rf octopole ion guide surrounded by a scattering cell, second quadrupole mass filter, and a pulse-counting detector. Both quadrupole mass filters use Extrel 9.5 mm trifilter rods, which were operated at 2.1 MHz to cover a mass/charge (m/z) range of 1−500.

Sample solution was prepared by dissolving 0.5 mM L-Tyr (99+ %, Acros) or L-Trp (99%, Acros) in HPLC grade methanol/water (4:1 vol. ratio) with 0.5 mM NaOH (reagent grade, Fisher) added to assist deprotonation. The solution was sprayed into the ambient atmosphere through an electrospray needle at a flow rate of 0.05 mL/h, and the electrospray needle was held at −2500 V relative to ground. Negatively charged droplets formed from electrospray were fed into a heated desolvation capillary assembly. The capillary was biased at −150 V relative to ground and heated to 160 °C. Charged liquid droplets and solvated ions underwent desolvation as they passed through the heated capillary, converting to gas-phase ions and transported into the source chamber. A skimmer was located 2.5 mm from the exit of the capillary, separating the

dx.doi.org/10.1021/jp303022b | J. Phys. Chem. B 2012, 116, 6369−6379

source chamber and the hexapole ion guide. The skimmer was biased at −20 V relative to ground, and the electric field between the capillary and skimmer removed remaining solvent molecules attached to ions by collision-induced desolvation. Negative ions emerging from the skimmer were passed into a rf hexapole ion guide at a pressure of ∼26 mTorr, resulting in collisional focusing and thermalization of internal and translational energies of ions.[65−67] As characterized by a collision-induced dissociation (CID) experiment,[43] the internal energy of primary ions could be described by a Maxwell−Boltzmann distribution at ∼310 K. Ions subsequently passed into the first quadrupole mass filter for mass selection. Mass-selected ions of $[Tyr\text{-}H]^-$ or $[Trp\text{-}H]^-$ were focused into an octopole ion guide. The octopole passes through a scattering cell filled with neutral reactant gas. The cell pressure was measured by a capacitance manometer (MKS Baratron 690 head and 670 signal conditioner). The ion guide minimizes losses of the reactant and product ions resulting from scattering. After passing through the scattering cell, any product ions and the remaining deprotonated amino acids drifted to the end of the octopole where they were mass analyzed and counted.

Initial kinetic energy distribution of the primary ion beam was determined using a retarding potential analysis (RPA),[68] i.e., the intensity of the primary ion beam was measured while sweeping the DC bias voltage applied to the octopole. The DC bias voltage also allowed control of the kinetic energy (E_{Lab}) of ions in the laboratory frame. E_{Lab} is converted into the collision energy (E_{col}) between ions and reactant gas molecules in the center-of-mass frame using $E_{col} = E_{Lab}m_{neutral}/(m_{ion} + m_{neutral})$, where $m_{neutral}$ and m_{ion} are the masses of neutral and ionic reactants, respectively. Ion beam intensities of $[Tyr\text{-}H]^-$ and $[Trp\text{-}H]^-$ were typically 4×10^5 ion/sec, and constant within 10%. Their initial kinetic energies were 0.15−0.25 eV, and the energy spreads were ∼0.4 eV which corresponds to an energy spread of ∼0.1 eV in the center-of-mass frame for the collision of $[Tyr\text{-}H]^-$ (or $[Trp\text{-}H]^-$) with $^1O_2$. Reaction cross sections were calculated from the ratio of product and reactant ion intensities, calibrated $^1O_2$ pressure, and the calibrated effective length of the scattering cell, using a Beer's Law relationship.[69]

$^1O_2$ was generated using the reaction of $H_2O_2 + Cl_2 + 2KOH \rightarrow O_2(X^3\Sigma_g^-$ and $a^1\Delta_g) + 2KCl + 2H_2O$.[70,71] This $^1O_2$ production method was used for ion−molecule reactions by Viggiano's group recently.[57,58,60−62] We adopted their procedure with some modifications.[39,49] Briefly, 20 mL of 35 wt. % H_2O_2 (Acros Organics) was mixed with 13 mL of 8 M KOH (>85%, Fisher) solution in a sparger that was immersed in a cold bath maintained at −19 °C, and the resulting solution was degassed. A continuous flow of He (research grade, T.W. Smith) was then introduced to the slushy H_2O_2/KOH mixture at a flow rate of 50 sccm to prevent freezing of the mixture. Finally, Cl_2 (≥99.5%, Sigma-Aldrich), at a flow rate of 2−3 sccm, was mixed with He in a gas proportioner and bubbled through the H_2O_2/KOH solution. All the Cl_2 reacted to form ground-state and excited O_2.[58] The resulting gas mixture passed through a cold trap kept at −70 °C to remove water vapor. Only $^3O_2$, $O_2(a^1\Delta_g)$, and He remained in the downstream gas flow and were introduced to ion−molecule collisions.

Before leaking into the scattering cell, the gases flowed through an emission cell to detect the emission of O_2 ($a^1\Delta_g \rightarrow X^3\Sigma_g^-$, $\nu = 0-0$) at 1270 nm.[72] The emission cell was continuously pumped through a pressure control valve to maintain a pressure at 15 Torr. This pressure was chosen to reduce the residence time and hence, the wall quenching of $^1O_2$ inside the cold trap, gas tubing, and emission cell. Emission from the cell was collected by a plano-convex BK7 lens, and passed through an optical chopper (SRS model SR540) and a 0.5 nm bandwidth interference filter centered at 1270 nm (Andover, blocked to 1.55 μm). Chopped emission was focused into a thermoelectrically cooled InGaAs detector (Newport 71887 detector and 77055 TE-cooler controller), and the signal was processed by a lock-in amplifier (SRS model SR830).

The detection system measured relative $^1O_2$ emission intensity. To determine absolute $^1O_2$ concentration, the detector was calibrated using the reaction cross sections of $HS^- + {}^1O_2 \rightarrow SO^- + OH$ at E_{col} of 0.1, 0.2, and 0.3 eV. HS^- was produced by ESI of a methanol/water (5:1 vol. ratio) solution containing a mixture of 0.5 mM H_2S (≥99.5%, Ricca Chemical) and 0.1 mM NaOH. HS^- anions had a similar initial kinetic energy distribution as that of deprotonated amino acids, and the reaction with $^1O_2$ was measured under the identical conditions used for deprotonated amino acids. The rate constant (k) for $HS^- + {}^1O_2 \rightarrow SO^- + OH$ was reported to be 0.54×10^{-10} $cm^3 \cdot molecule^{-1} \cdot s^{-1}$ by Viggiano et al.[61] Cross sections (σ) at different E_{col} can then be calculated using $\sigma = k/\nu_{rel}$, where the relative ion−molecule velocity $\nu_{rel} = [2E_{col}/(m_{neutral}m_{ion}/(m_{ion} + m_{neutral}))]^{1/2}$.[69] The calibration indicates that the maximum emission intensity detected corresponds to a 5−10% $^1O_2$ yield in the total oxygen flow, which is close to the values reported by Viggiano et al.[57,59,62] Since the emission intensity linearly depends on $^1O_2$ concentration, the change of $^1O_2$ concentration during the experiment could be monitored by measuring the emission. $^1O_2$ pressure in the scattering cell is the product of the total gas pressure in the scattering cell, the percent of Cl_2 in the Cl_2 /He flow, and the $^1O_2$ concentration in the oxygen product.

The collision cross section ($\sigma_{collision}$), taken as the greater of the ion-induced dipole capture cross section ($\sigma_{capture}$)[73] and hard-sphere collision cross section ($\sigma_{hard\text{-}sphere}$), is about 40−50 $Å^2$ for $[Tyr\text{-}H]^- + O_2$ and 60−95 $Å^2$ for $[Trp\text{-}H]^- + O_2$ in the studied E_{col} range. $\sigma_{hard\text{-}sphere}$ is calculated from the orientation-averaged contact radii of deprotonated amino acid and O_2 and exceeds $\sigma_{capture}$ for $[Tyr\text{-}H]^- + O_2$ at $E_{col} > 0.3$ eV, and that for $[Trp\text{-}H]^- + O_2$ at $E_{col} > 0.1$ eV. The pressure of O_2/He in the scattering cell was maintained at 0.3−0.4 mTorr, which contained ∼5% of O_2. This pressure range was chosen to provide reasonable intensities of product ions, while keeping multiple-collision effects to a minimum level. In this range of pressure, the probability of $[Tyr\text{-}H]^-$ and $[Trp\text{-}H]^-$ undergoing a single-collision with O_2 is <3%, and that of double collisions is <0.1%. Note that $[Tyr\text{-}H]^-$ and $[Trp\text{-}H]^-$ also collided with He gas within the scattering cell, with a single-collision probability of 15−20%, and a double-collision probability of 3−6%. However, the light neutral-heavy ion combination makes these collisions insignificant compared to those with O_2.

The intensity of $^1O_2$ emission was monitored continuously during the whole experiment, and the signal variation (controlled to be within 20%) was corrected for in calculating reaction cross section. RPA measurements of primary ions were performed before and after each experiment to check the initial kinetic energy of the primary ion beam. As a check on reproducibility, the entire experiment was repeated several times and each time we cycled through different collision energies. The data presented are averages of several independent data sets. Based on the reproducibility of the cross section measurements taken over a two-month period, we estimate that the relative error is ∼25%. To check the reactivity

dx.doi.org/10.1021/jp303022b | J. Phys. Chem. B 2012, 116, 6369−6379

of $[Tyr-H]^-$ and $[Trp-H]^-$ toward $^3O_2$ and He, control experiments were performed under the same conditions except that Cl_2 was replaced by O_2 gas at the same flow rate.

B. Computational Methods. To aid in reaction coordinate interpretation, DFT electronic structure calculations were performed at the B3LYP level of theory with various basis sets including 6-31+G*, 6-311+G*, and 6-311++G**, using Gaussian 09.[74] Note that due to the mixing of open-shell and closed-shell characteristics of $^1O_2$, standard DFT calculations lead to large errors in the electronic excitation energy of $^1O_2$.[75] In our calculations, the DFT energy of $^1O_2$ was obtained by adding the experimental excitation energy of 0.98 eV[72] to the DFT energy of $^3O_2$. All geometries were optimized by calculating force constants at every step. Vibrational frequencies and zero-point energies (ZPE) were scaled by a factor of 0.955 and 0.981,[76] respectively. All of the transition states (TSs) found were verified as first-order saddle points by frequency calculations, and the vibrational mode with imaginary frequency corresponds to the reaction pathway. When necessary intrinsic reaction coordinate (IRC) calculations were used to determine which minima are connected by a particular TS. The details of the geometries for complexes, TSs, and products are available by request to the corresponding author. RRKM calculations were done with the program of Zhu and Hase,[77] using its direct count algorithm, and scaled frequencies and energetics from DFT calculations.

To validate the importance of the steps identified in the reaction coordinate, quasi-classical, direct dynamics trajectory simulations were conducted for $[Tyr-H]^- + {}^1O_2$. The dynamics program VENUS99[78] was used to set up trajectory initial conditions, and the updating Hessian method[79] in Gaussian was used to propagate each trajectory. On the basis of the overall level of agreement with high level benchmark results and computational speed, we chose B3LYP/4−31G* for calculating trajectories. Trajectory integrations were performed with a step size of 0.25 $amu^{1/2}$ bohr (corresponding to a step size of ∼0.5 fs in trajectory integration), which conserved the total energy to better than 10^{-4} Hartree. The SCF = XQC option was adopted during trajectory integration so that a quadratically convergent Hartree−Fock (QC-SCF) method[74,80] was used in case the usual, but much faster, first-order SCF method did not converge within the allotted number of cycles. E_{col} was set at 0.75 eV for simulations.

The purpose of trajectory simulations is to probe the gross features of the $[Tyr-H]^- + {}^1O_2$ collisions, thus all 100 trajectories were calculated at the impact parameter b of 0.5 Å, rather than randomly sampling the b distribution. The initial conditions of the reactants were chosen to mimic the experimental conditions. Because $[Tyr-H]^-$ ions were thermalized in the experiment, their initial vibrational and rotational energies in trajectories were sampled from Boltzmann distributions at 300 K. Similarly, 300 K was used for $^1O_2$ rotational and vibrational temperature. Quasi-classical initial vibrational state was simulated by giving each reactant atom displacement from equilibrium and momentum appropriate to the initial rovibrational state, with random phases for different modes. Both $[Tyr-H]^-$ and $^1O_2$ have zero-point energy in all vibrational modes. Randomly oriented $[Tyr-H]^-$ and $^1O_2$ were given relative velocities corresponding to the simulated collision energy. All trajectories started with an initial center-of-mass reactant separation of 7.5 Å, and were terminated either when the distance between the final products exceeded 7.0 Å, or after 3000 steps. Trajectories were calculated on an Intel core 2 quad (3.0 GHz)-based 64 bit Linux computational cluster, and each trajectory took 1000−1500 CPU hours. gOpenMol[81] was used for trajectory visualization. Analysis of individual trajectories and statistical analysis of the trajectory ensemble were done with programs written for these purposes, as described previously.[43,82,83]

III. RESULTS AND DISCUSSION

A. Reaction Cross Sections. For the reaction of $[Tyr-H]^-$ (m/z 180) + $^1O_2$, product ions were observed at m/z 134 over the collision energy range of 0.1−1.0 eV, corresponding to elimination of H_2O_2 and CO_2 from the system. The exoergicity of the reaction is 1.83 eV calculated at B3LYP/6-31+G* (vide infra). In principle, the product ions of m/z 134 could be attributed to elimination of a formic acid molecule from $[Tyr-H]^-$. We discount this possibility because, as rationalized in reaction coordinate calculations, the corresponding reaction pathway involves a much higher energy barrier. The reaction cross section is given in Figure 1, as a function of the center-of-mass E_{col}. Due to the uncertainties in determining $^1O_2$ absolute concentration, we state that the absolute uncertainty in the cross section measurement could be as large as a factor of 2. This source of uncertainty does not affect the relative cross section, i.e., the collision energy dependence, which is our primary interest in the study. The relative uncertainty is estimated to be ∼25%.

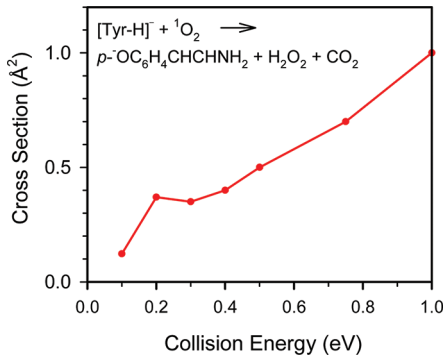

Figure 1. Cross section for the reaction of $[Tyr-H]^-$ with $^1O_2$, as a function of center-of-mass collision energy.

Our result shows a threshold-like behavior at low collision energies, raising the possibility of an energy barrier in excess of the reactant energy. Ordinarily, we would fit the E_{col} dependence of the cross section to extract the true threshold energy, i.e., convoluting a model "true" $\sigma(E_{col})$ function with appropriate experimental broadening factors and kinetic shift.[43] For "true" $\sigma(E_{col})$ function, we used the modified line-of-centers model.[84,85] However, the present system has large internal energy distributions and may involve various conformations of $[Tyr-H]^-$. In addition, the amplitude of the cross section is very small and does not reach zero at lowest E_{col}. We, therefore, just crudely extrapolate the raw cross section to estimate the appearance energy which is of ∼0.1 eV. Assuming the internal and translational energy distributions of $[Tyr-H]^-$ ions are close to what we measured for Na^+(proline),[43] the true reaction threshold should be close to 1.0 eV. Although the endothermic E_{col} dependence of the cross section does not rule out the existence of a barrierless pathway strongly inhibited by dynamical constraints at low E_{col}, the estimated threshold seems in good accord with our calculated

dx.doi.org/10.1021/jp303022b | J. Phys. Chem. B 2012, 116, 6369−6379

reaction coordinate to be discussed below. In either case, the low reactivity of $[Tyr\text{-}H]^-$ is consistent with the solution-phase results measured at the pH range between 5.7 (i.e., p*I* of Tyr) and 8.[20,21]

At higher collision energies, product ions were also observed at *m*/*z* 163, 136, 119, and 93. These four product ion masses correspond to elimination of NH_3, CO_2, and concomitant loss of (NH_3 + CO_2) and (CH_2CHNH_2 + CO_2), respectively, from $[Tyr\text{-}H]^-$. These product ions are attributed to CID[86−88] and were observed upon collisions of $[Tyr\text{-}H]^-$ with ground-state O_2 and Ar, too. Among these CID product channels, *m*/*z* 163 is largely dominant. Product ions of *m*/*z* 134, on the other hand, were not obviously observed with ground-state O_2, Ar, or He and cannot be attributed to CID. There is no sign of elimination involving generation of *p*-$HOC_6H_4CH_2^-$.

For the reaction of $[Trp\text{-}H]^-$ (*m*/*z* 203) + $^1O_2$, product ions were observed at *m*/*z* 157. Similar to that for $[Tyr\text{-}H]^-$ + $^1O_2$, this product channel corresponds to elimination of H_2O_2 and CO_2 from a reaction intermediate. The intensity of *m*/*z* 157 due to the reaction with $^3O_2$ was less than 1%; thus, the reaction with $^3O_2$ is negligibly small in comparison to that with $^1O_2$. In addition, CID product ions were observed at *m*/*z* 186, 159, 142, 116, and 74 at high E_{col}, due to elimination of NH_3, CO_2, (NH_3 + CO_2), (CH_2CHNH_2 + CO_2), and the side chain from $[Trp\text{-}H]^-$, respectively.[86,87] These CID product ions were also observed in the control experiments with $^3O_2$, He and Ar, and therefore are not relevant to $^1O_2$ chemistry. The cross section for the product channel of *m*/*z* 157 is shown in Figure 2

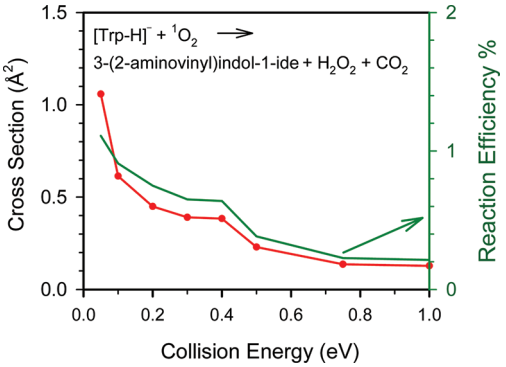

Figure 2. Cross section for the reaction of $[Trp\text{-}H]^-$ with $^1O_2$, as a function of center-of-mass collision energy. Also shown is the estimated reaction efficiency.

over the center-of-mass E_{col} range from 0.05 to 1.0 eV, together with the reaction efficiency estimated as $\sigma_{reaction}/\sigma_{collision}$. The cross section is significant only at the lowest energies and is strongly suppressed by E_{col}. The reaction efficiency is only 1.1% at E_{col} = 0.05 eV, dropping to ∼0.4% at E_{col} = 0.5 eV and 0.2% at E_{col} above 1.0 eV. One interesting mechanistic question is why the reaction efficiency is so low, despite the fact that the reaction is exothermic. The low reaction efficiency may reflect the competition between chemical reaction and physical quenching of $^1O_2$ by Trp.

Note that, as rationalized in the next section, $TyrO^-$ (i.e., the phenoxide structure of $[Tyr\text{-}H]^-$) and $TrpN^-$ (i.e., the deprotonated indole structure of $[Trp\text{-}H]^-$) were not present in our experiments, and the reactions of $[Tyr\text{-}H]^-$ and $[Trp\text{-}H]^-$ occur exclusively in their carboxylate anion structure (i.e., $TyrCO_2^-$ and $TrpCO_2^-$). Electron detachment energies are 3.55[89] and 3.53 eV for $TyrCO_2^-$ and $TrpCO_2^-$, respectively; both of which are beyond the E_{col} range of 0.05−1.0 eV used in our experiment. Therefore, we can disregard the detachment of the excess electron from $TyrCO_2^-$ and $TrpCO_2^-$ during initial collisions. Assuming the $^1O_2$ electronic excitation energy and O_2 electron affinity (0.45 eV)[90] can all be used to drive reactions, charge transfer between these carboxylate anions and $^1O_2$ is endothermic by 2.1 eV, and therefore cannot occur in our E_{col} range, either.

B. Reaction Mechanisms. One issue for interpretation of amino acid chemistry is that amino acids exist in various geometric conformations resulting from the flexibility of their structures. In addition, Tyr has two sites for deprotonation, i.e., the backbone carboxylic acid group and the side-chain phenolic group. Consequently, there exist carboxylate and phenoxide anion structures for $[Tyr\text{-}H]^-$. Considering all possible orientations for the C^α−C^β bond, −COOH, and phenolic −OH, we have located eighteen conformations for $[Tyr\text{-}H]^-$ at B3LYP/6-311+G* level of theory. Six of these belong to the carboxylate structure (i.e., $TyrCO_2^-$), and the remaining belong to the phenoxide structure (i.e., $TyrO^-$). They are each divided into several subgroups, differing by the orientation of the amino acid group with respect to the plane of the phenolic ring. Their structures and relative energies (with respect to $TyrO^-$_1a, the lowest energy conformation at B3LYP/6-311+G*) are summarized in Figure 3. In the figure, each illustrated structure of $TyrCO_2^-$ represents a pair of conformers, corresponding to two different orientations of the phenolic −OH on the side chain, with small energy differences of less than 30 meV. All

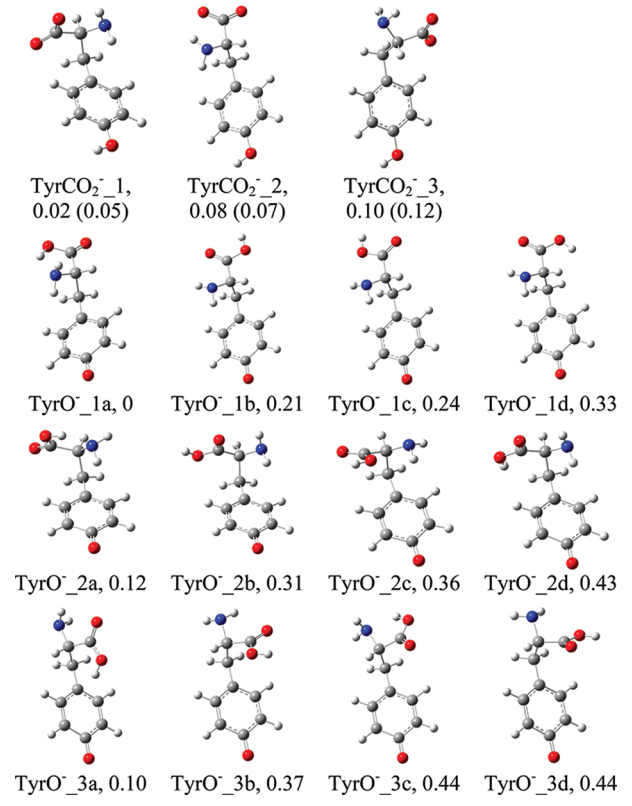

Figure 3. Low-lying conformations of $[Tyr\text{-}H]^-$ calculated at B3LYP/6-311+G*. Their relative energies at 0 K (eV, including ZPE) are indicated below each structure. Note that the rotation of the phenolic −OH results in a pair of stable $TyrCO_2^-$ conformations, only one of which is illustrated, and the energy of the other is given in parentheses.

dx.doi.org/10.1021/jp303022b | J. Phys. Chem. B 2012, 116, 6369−6379

$TyrCO_2^-$ conformations contain a $NH_2\cdots O{=}C$ intramolecular hydrogen bond with a distance of 2.08 - 2.25 Å between the O atom and the closer H of NH_2. Of the $TyrO^-$ conformations, the low-lying structures (i.e., $TyrO^-$_1a, 2a and 3a) contain a *trans*- configuration of the carboxylic acid group, and either an intramolecular hydrogen bond of $OH\cdots NH_2$ for $TyrO^-$_1a and 2a with a distance of 1.85 Å from the hydroxyl H to the N atom, or an intramolecular hydrogen bond of $NH_2\cdots O{=}C$ for $TyrO^-$_3a with a distance of 2.38 Å from the O atom to the closer H of NH_2. $TyrO^-$ anions have many high energy-lying conformations, in which the excess charge on the phenoxide ring is delocalized to the aromatic ring.[89] Our calculated conformations are consistent with literature results.[89,91]

The difference in the acidity of the most stable $TyrCO_2^-$ and $TyrO^-$ structures is only 20 meV. This poses a question of which structure would exist in our ESI ion source. Tian et al.[92] claimed that ESI of Tyr from 3:1 (v:v) methanol/water solution produced a 70:30 mixture of phenoxide and carboxylate anions at equilibrium in the gas phase, as confirmed by photoelectron spectra.[89] In contrast to Tian et al.'s findings, using a similar ESI solution, Oomens et al.[93] detected only a pure carboxylate structure in the gas phase from infrared multiphoton dissociation (IRMPD) spectroscopy. According to Bradford et al.[94] and Couldwell et al.,[88] phenoxide anions have characteristic CID products ions at m/z 74 (backbone), 106 (p-$^-OC_6H_4CH_2$), and 107(p-$^-OC_6H_4CH_3$). However, these fragment ions were either absent or extremely minor in our control experiment of $[Tyr\text{-}H]^-$ with Ar; we therefore concluded that our ESI source produced only the carboxylate anions for the reaction with $^1O_2$.

We also applied the grid search method to find the global minimum of $[Trp\text{-}H]^-$ in its conformation landscape. Similar to Tyr, deprotonated Trp anions have two structures, i.e., $TrpCO_2^-$ due to the deprotonation of the backbone carboxylic acid group and $TrpN^-$ due to the deprotonation of the indole −NH group. A set of $TrpCO_2^-$ conformations is depicted in Figure 4, of which the energy difference is within 0.18 eV. $TrpCO_2^-$ conformations are all stabilized by a hydrogen bond between the amino H atom and the carboxyl O atom, with an interaction distance of 2.0−2.57 Å. The group of $TrpN^-$ conformations lies 0.31−0.54 eV higher in energy with respect to $TrpCO_2^-$ and is less likely to be populated at experimental temperature of 300 K. Our lowest energy conformation of $[Trp\text{-}H]^-$ is in agreement with previous calculations using molecular dynamics simulations followed by reoptimization at the MP2/6-311++G** level of theory.[95]

In the subsequent reaction coordinate calculations and mechanism discussion, $[Tyr\text{-}H]^-$ and $[Trp\text{-}H]^-$ will be particularly referred to their lowest-energy conformers, $TyrCO_2^-$_1 and $TrpCO_2^-$_1a, respectively. Note that the structures of $TyrCO_2^-$_1 and $TrpCO_2^-$_1a correspond excellently with the IRMPD spectra of gas-phase $[Tyr\text{-}H]^-$ and $[Trp\text{-}H]^-$, respectively.[93] It is certainly possible that interconversion between different rotamers of $TyrCO_2^-$ or $TrpCO_2^-$ might occur during collisions. However, it seems less likely that different conformations of $TyrCO_2^-$ or $TrpCO_2^-$ would significantly alter their reaction coordinate, as confirmed in present trajectory simulations of $[Tyr\text{-}H]^- + {}^1O_2$, as well as in our trajectories simulations of $TyrH^+ + {}^1O_2$,[43] $MetH^+ + {}^1O_2$,[49] and $CysH^+ + {}^1O_2$.[39]

1. [Tyr-H]$^-$ + $^1O_2$. 1.1. Reaction Coordinate. Product ions of m/z 134 could be due to concomitant elimination of either ($HCO_2H + O_2$) or ($H_2O_2 + CO_2$) from a reaction intermediate

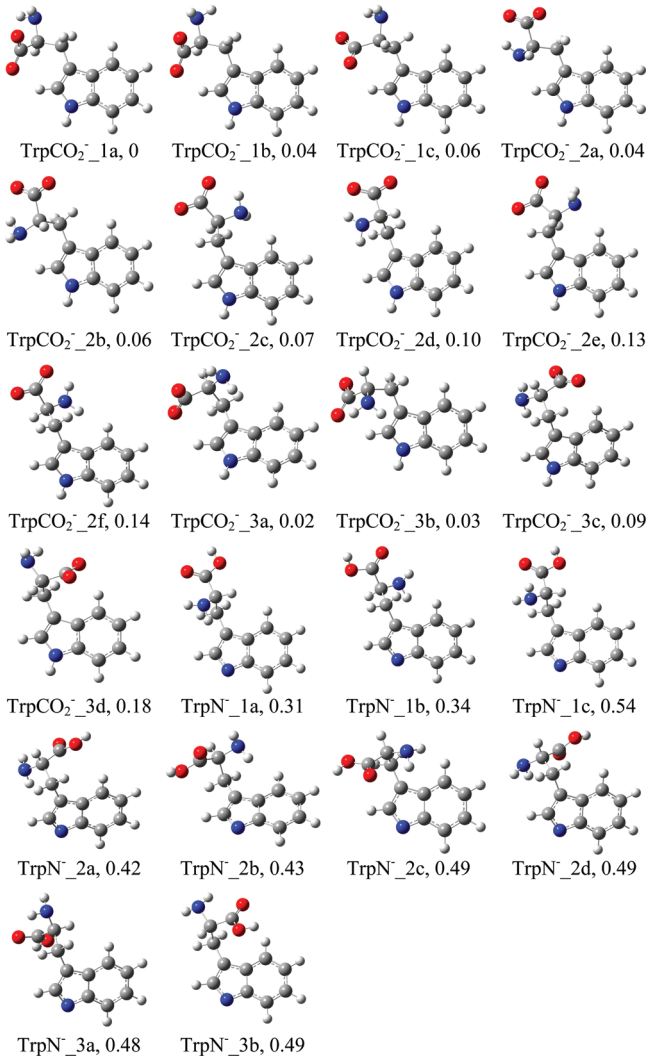

Figure 4. Low-lying conformations of $[Trp\text{-}H]^-$ calculated at B3LYP/6-311++G**. Their relative energies at 0 K (eV, including ZPE) are indicated below each structure.

complex. DFT calculation results for both possibilities are included in Figure 5, with the reactants shown at zero energy. Energetics are driven from a combination of B3LYP/6-31+G* calculations and the experimental value of $^1O_2$ excitation energy. Several weakly bound complexes (precursor complexes 1 and 2) and covalently bound complexes (including endoperoxide and hydroperoxides) were found, and their structures are depicted in the figure. Precursor complexes 1 and 2 can be characterized as reactant-like in structure. Precursor 1 has a hydrogen bond between phenolic H and O_2 moiety with a H···O distance of 1.83 Å, and a binding energy of 0.57 eV with respect to the reactants. Precursor 2 is electrostatically bound with no covalent or hydrogen bond. It has O_2 oriented parallel to the phenol ring with the closest distance between O_2 and the phenol ring being 2.5 Å, and bound by 0.27 eV with respect to the reactants. Presumably, these two precursor complexes can interconvert facilely. Because no rearrangement is required to form these precursor complexes, it is less likely that there would be significant energy barriers to inhibit their formation. This conclusion has been confirmed by a relaxed potential energy scan running along the dissociation of these complexes back to separated reactants. Note that these precursor complexes are

dx.doi.org/10.1021/jp303022b | J. Phys. Chem. B 2012, 116, 6369−6379

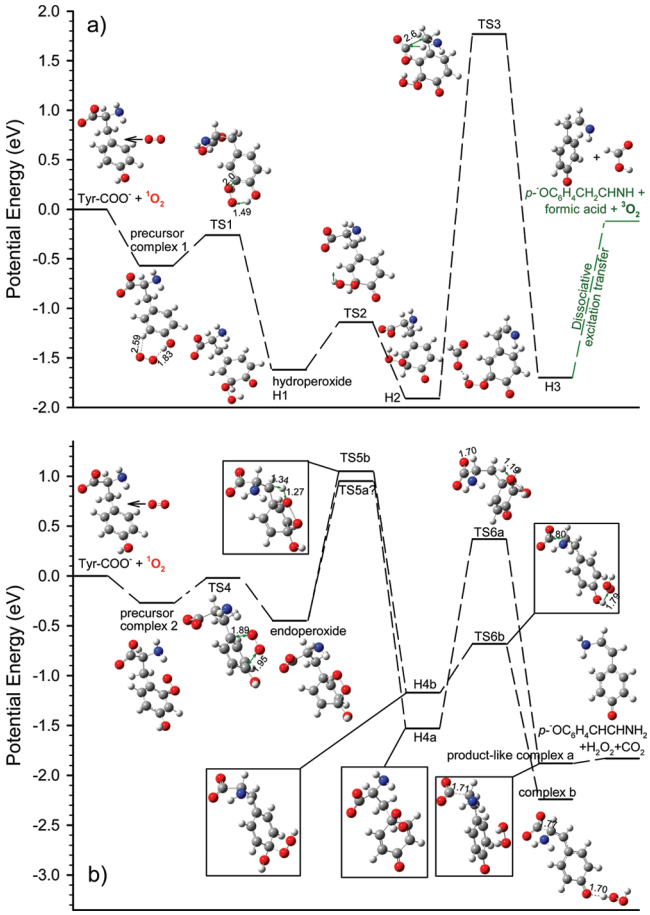

Figure 5. Schematic reaction coordinate for $[Tyr\text{-}H]^-$ + $^1O_2$. Energies of complexes, TSs, and products, relative to reactants, are derived from B3LYP/6-31+G* results, including ZPE. The bond distances are shown in angstroms. For TSs, vibrational modes corresponding to the imaginary frequencies are indicated by displacement vectors.

rather floppy and have no well-defined geometries, with a large amplitude of intermolecular motions with respect to the rotation of amino acid and O_2 moieties, as shown by the harmonic hindered rotor frequencies of just 64 and 90 cm^{-1}, respectively. They allow repeated encounters between $[Tyr\text{-}H]^-$ and $^1O_2$, increasing the probability of interconverting to a covalently bound endoperoxide and/or hydroperoxide. For these reasons, they are referred to as "precursor" complexes.

In Figure 5a, a reaction pathway leading to concomitant loss of formic acid and ground-state O_2 is proposed. Precursor complex 1 interconverts to hydroperoxide H1 via the transition state TS1. Hydroperoxide H1 subsequently interconverts to an analogue H2 via TS2. Both H1 and H2 have the phenolic H atom abstracted by the peroxide group, with the difference being in the orientation of -OOH with respect to the amino acid backbone. The -OOH group of H2 is much closer to the carboxyl O atom than that of H1. H2 undergoes intramolecular H atom from the amino group to the carboxyl C atom and consequently breaks the C^{α}–C^{β} bond, producing a hydrogen-bonded complex H3 via a high and tight TS3. H3 may undergo subsequent dissociation driven by the excitation energy of $^1O_2$, the so-called "dissociative excitation energy transfer".[39,60] In this process, H3 undergoes three-body dissociation to p-$^-OC_6H_4CH_2CHNH$ (i.e., 4-(2-iminoethyl)phenolate), formic acid, and ground-state oxygen. Assuming all of the $^1O_2$ excitation energy could be used to drive the dissociation of H3, the calculated ΔH_{rx} is 0.12 eV exothermic. Similar dissociative excitation transfer was observed in $CysH^+$ + $^1O_2$ and $TrpH^+$ + $^1O_2$.[39] However, the reaction path in Figure 5a involves a high and restricted barrier TS3 of 1.8 eV relative to the separated reactants and becomes both entropically constrained and energetically inaccessible at our collision energies of 0.1−1.0 eV. We note that the excitation energy of the triplet state $^3[Tyr\text{-}H]^-$ is calculated to be 3.32 eV, therefore electronic energy transfer from $^1O_2$ to $^3[Tyr\text{-}H]^-$ via intersystem crossing is not feasible, either. The system must seek a more energetically favorable dissociation path to product ions of m/z 134.

In solution, $^1O_2$-mediated photooxidation of Tyr (in its zwitterionic structure)[16,17] was initialized by formation of an endoperoxide which underwent rapid ring-opening to give a hydroperoxide situated at the C1 ring-position (i.e., para to the phenolic group), and the resulting hydroperoxide which slowly decayed at low temperature was characterized experimentally.[16,17] Solution-phase mechanism provides us a guide for the construction of an alternative reaction pathway in the gas phase, as illustrated in Figure 5b. Consistent with the solution-phase mechanism, the reactants form precursor complex 2 upon collisions, which interconverts to an endoperoxide via TS 4. The endoperoxide has oxygen atoms bonded to C1 and C4 atoms of the phenol ring, with a binding energy of 0.45 eV. Consequently, C1 and C4 are displaced from the ring plane toward O_2. The endoperoxide subsequently interconverts to two different hydroperoxides H4a and H4b, with the −OOH located at the C1 or C4 atom of the phenol ring, respectively. We were not able to locate a transition state TS5a connecting the endoperoxide to H4a. But a relaxed potential energy scan along the H transfer from the phenolic O to the peroxide O results in an energy barrier of <1 eV with respect to the reactants. The transition state TS5b, located between the endoperoxide and H4b, was calculated to be 1.05 eV above the reactants. Both H4a and H4b can serve as an intermediate for elimination of H_2O_2 + CO_2, i.e., each of them goes through intramolecular H transfer from $-C^{\beta}H_2$ (via TS6a) or phenolic −OH (via TS6b) to the −OOH group, leading to a corresponding product-like complex. The vibrational mode associated with the imaginary frequency of TS6a/TS6b corresponds to intramolecular H transfer accompanied by decarboxylation of the backbone. Consequently, product-like complexes a and b have the CO_2 and H_2O_2 moieties electrostatically- or hydrogen-bonded to the remaining ionic structure. ΔH_{rx} for the production of p-$^-OC_6H_4CHCHNH_2$ (i.e., 4-(2-aminovinyl)phenolate) + H_2O_2 + CO_2 is calculated to be −1.83 eV. According to Mulliken charge analysis, the negative charge of p-$^-OC_6H_4CHCHNH_2$ is mostly located on the phenolic O atom (δ^- = 0.71).

Based on a previous modeling of the E_{col} dependence of Na^+(proline) CID cross section measured using the same instrument,[43] we sense that the energy barriers of TS5a/5b are in reasonable agreement with the experimentally observed threshold for $[Tyr\text{-}H]^-$ + $^1O_2$ (Figure 1). Therefore, both these two routes, i.e., reactants → precursor 2 → TS4 → endoperoxide → TS5a (or TS5b) → H4a (or H4b) → TS6a (or TS6b) → product-like complex a (or b) → p-$^-OC_6H_4CHCHNH_2$ + H_2O_2 + CO_2, are likely to participate in the reaction, leading to concerted elimination of neutral H_2O_2 and CO_2, and producing product ion of p-$^-OC_6H_4CHCHNH_2$. In this context, it is interesting to note the fate of the fraction of precursor complexes/

dx.doi.org/10.1021/jp303022b | J. Phys. Chem. B 2012, 116, 6369−6379

endoperoxides which formed during collisions but did not lead to reactions. In the study of $TyrH^+ + {}^1O_2$,[43] we found that collisions lead to overwhelming formation of various endoperoxides (with efficiency over 90% at $E_{col} \leq 0.1$ eV), and these endoperoxides act as intermediates for physical quenching of $^1O_2$. Only a small fraction of collisions produce hydroperoxide intermediates, which eventually lead to elimination of H_2O_2. A similar scenario may occur for $[Tyr\text{-}H]^- + {}^1O_2$, i.e., physical quenching of $^1O_2$ occurs via the intermediacy of precursor 2/endoperoxide. No other low energy pathways were found leading to the formation of $p\text{-}^-OC_6H_4CHCHNH_2$, although we certainly cannot rule out the possibility that such pathways exist.

1.2. Direct Dynamics Trajectory Simulations. Trajectories were run at E_{col} = 0.75 eV and b = 0.5 Å. Roughly 90% of all one hundred trajectories belong to direct nonreactive scattering, resulting in conversion of some collision energy into vibrational and rotational energy. The remaining trajectories formed electrostatically bound weak complexes, i.e., precursor complex 2 in Figure 5b. Figure 6 demonstrates

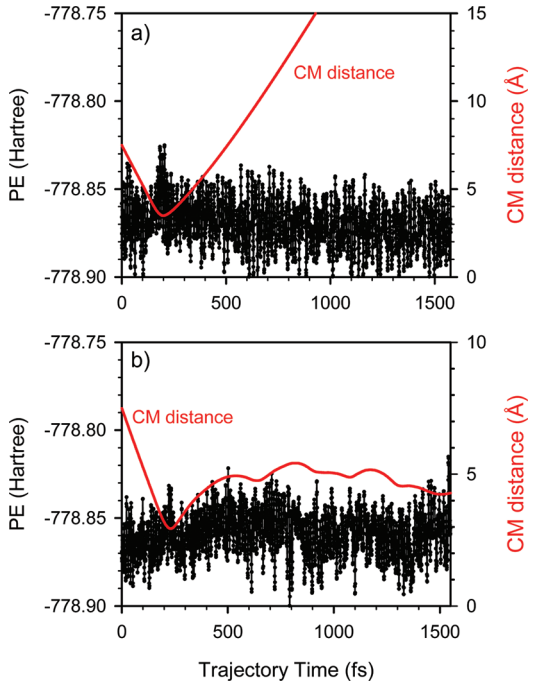

Figure 6. Representative plots of (a) a nonreactive trajectory and (b) a precursor complex-forming trajectory at E_{col} = 0.75 eV, showing the variation of potential energy and center-of-mass distance between $[Tyr\text{-}H]^-$ and O_2 moieties during the trajectory.

two trajectories representative of nonreactive and complex-forming collisions, respectively. The plots show changes of CM distance and potential energy (PE) during each trajectory. The CM distance is the distance between the centers of mass of the collision partners. The top frame of Figure 6 shows a direct, nonreactive scattering, with only one turning point in the relative motion of the reactant centers of mass, i.e., there is no sign of mediation by a complex in this collision. The time scale of the collision is somewhat arbitrary, but three numbers are relevant. The time between trajectory starts and the onset of strong interaction, which depends on reactant orientation, is around 150 fs. The time for reactant approach within 5 Å of center-of-mass distance is around 240 fs. More importantly, the time period during which $[Tyr\text{-}H]^-$ and $^1O_2$ interact strongly is around 100 fs as shown by the potential energy spike beginning at $t \approx 150$ fs during the trajectory. The bottom frame of Figure 6 illustrates a precursor complex-forming trajectory, with similar reactant approach time. The oscillations in PE reflect the vibrations of the reactants or products, including ZPE. No obvious potential barrier was observed during the formation of the complex. The precursor complex is assumed to decay back to reactants or interconvert to an endoperoxide, but it is not practical to propagate the complex-forming trajectories long enough to observe its decay. In fact, none of the complex-forming trajectories decay back to the reactants before the termination of the trajectory (~1.5 ps). This suggests that the lifetime of trajectory-formed precursor complexes is longer than 1.5 ps. For comparison, the classical rotational period of the precursor complex using the average angular momentum is 2.0 ps at E_{col} = 0.75 eV. We also calculated the direct reaction time, taken as the time for undeflected reactants to fly past each other over a distance of 10 Å. This "fly by" time is 0.43 ps at E_{col} = 0.75 eV. The lifetime of the precursor complex is thus longer than the "fly by" time, and at least comparable to the complex rotational period. The implication is that the precursor complex is sufficiently long-lived to mediate the reaction.

It was found that complex-forming trajectories occur only in a restricted range of reactant orientations with the O_2 moiety approaching the phenolic ring at the collision point. At b = 0.5 Å, only less than half of all collisions have the favorable reactant orientation at their center-of-mass turning point, and ~20% of these form complexes. The remaining collisions have O_2 attack the backbone, which lead to nonreactive scattering. Therefore, we may expect the reaction efficiency at high E_{col} is to some extent controlled by the impact parameter and collision orientation. Similar collision orientation dependence was observed in trajectories of $TyrH^+ + {}^1O_2$.[43] The reaction of $TyrH^+ + {}^1O_2 \rightarrow [Tyr\text{-}H]^+ + H_2O_2$ occurs either via direct abstraction of two H atoms by O_2 from $TyrH^+$ or through a hydroperoxide-mediated mechanism. Both mechanisms require reactants to be well-oriented, and the chance of having a favorable orientation at the time when the reactants start to collide is less than 20%.

2. $[Trp\text{-}H]^- + {}^1O_2$. 2.1. Reaction Coordinate. DFT calculated reaction coordinate for $[Trp\text{-}H]^- + {}^1O_2$ is summarized in Figure 7. Similar to $^3[Tyr\text{-}H]^-$, triplet state $^3[Trp\text{-}H]^-$ has an excitation energy (2.75 eV) much higher than that of $^1O_2$, therefore the involvement of $^3[Trp\text{-}H]^-$ in the reaction can be overlooked over our energy range. Two weakly bound precursor complexes were found that might be important in mediating the reaction. To differentiate the precursor complexes for $[Tyr\text{-}H]^- + {}^1O_2$ and $[Trp\text{-}H]^- + {}^1O_2$, we include the reactant formula in the acronym, e.g., precursor complex ($[Trp\text{-}H]^-$), where necessary for clarity. Precursor complexes ($[Trp\text{-}H]^-$) 1 and 2 have similar structures except that the O_2 moiety approaches the indole plane from opposite directions. Both complexes have a distance of 2.2–2.6 Å between O_2 and the indole ring plane; consequently they have a nearly equal binding energy of 0.56–0.57 eV relative to the reactants, which are similar to or slightly higher than those found for precursor complexes ($[Tyr\text{-}H]^-$). As in the case of $[Tyr\text{-}H]^- + {}^1O_2$, precursors complexes ($[Trp\text{-}H]^-$) could interconvert to strongly bounded hydroperoxides H1, H2, H3, and H4 via various TSs, as indicated in Figure 7. All these hydroperoxides are formed by H abstraction from −NH of the indole ring. H1, H2, and H3 have the hydroperoxide attached

dx.doi.org/10.1021/jp303022b | J. Phys. Chem. B 2012, 116, 6369–6379

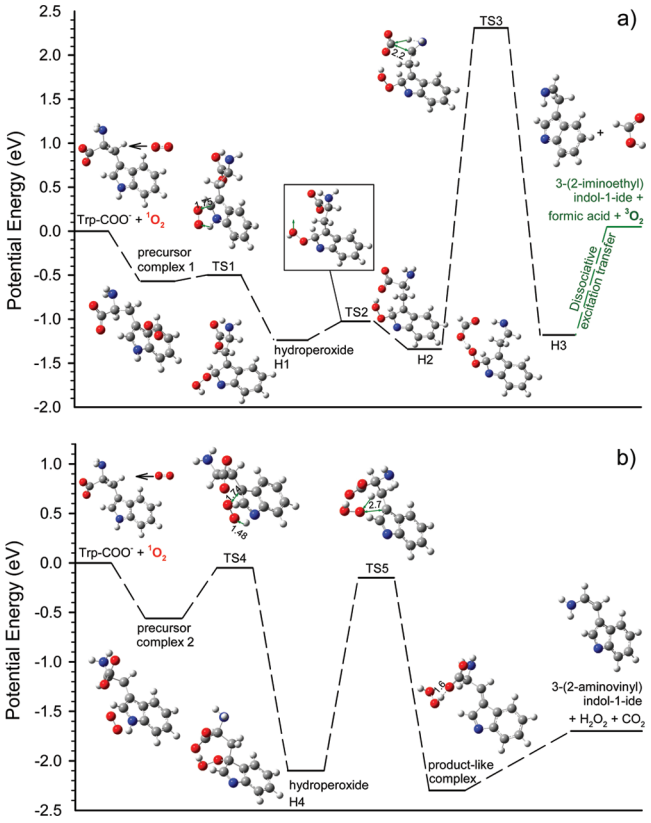

Figure 7. Schematic reaction coordinate for $[Trp\text{-}H]^-$ + $^1O_2$. Energies of complexes, TSs, and products, relative to reactants, are derived from B3LYP/6-31+G* values, including ZPE. The bond distances are shown in angstroms. For TSs, vibrational modes corresponding to the imaginary frequencies are indicated by displacement vectors.

to C2 of the indole ring, while H4 has the hydroperoxide anchored to the C1 position.

Figure 7a proposes a reaction pathway yielding product ion 3-(2-iminoethyl)indol-1-ide, formic acid and ground state O_2, via a dissociative excitation energy transfer mechanism, a similar mechanism as we have proposed for $[Tyr\text{-}H]^-$ + $^1O_2$ in Figure 5a. It is worth noting that we have observed the dissociative excitation energy transfer in the reaction of $TrpH^+$ + $^1O_2$ recently.[39] Should dissociative excitation transfer occur for $[Trp\text{-}H]^-$ + $^1O_2$ as outlined in Figure 7a, the reaction ΔH_{rx} is slightly endothermic by 0.05 eV; however, the reaction involves an extremely high and tight transition state TS3 (2.31 eV above the reactants) and can therefore be excluded. A more energetically favorable reaction pathway is established in Figure 7b, i.e., reactants → precursor 2 → TS4 → H4 → TS5 → product-like complex →3-(2-aminovinyl)indol-1-ide + H_2O_2 + CO_2, without any activation barriers above the reactants. In TS5, the −O*OH group is dissociating from the C1 position of indole, and simultaneously a H atom is transferring from the C^β atom of the backbone to O*. In the resulting product-like complex, the H_2O_2 moiety is hydrogen bound to the carboxyl group. We have attempted to locate a transition state leading to decarboxylation of the product-like complex. However, all guessed geometries converged to a stable structure. We found that, once we removed the H_2O_2 moiety, the remaining structure spontaneously dissociated into product ion 3-(2-aminovinyl)indol-1-ide and CO_2 during geometry optimization (presumably because of the energy gained by formation of a -C^α=C^β- bond in product ion). Based on this calculation result, we don't expect any reverse barrier located in the product exit channel. The enthalpy of reaction for the production of 3-(2-aminovinyl)indol-1-ide is calculated to be −1.70 eV. In 3-(2-aminovinyl)indol-1-ide, the negative charge is partitioned to the indole N and two neighboring C atoms.

2.2. RRKM Modeling. To evaluate whether the complexes and the reaction path identified in Figure 7b could account for the experimental observation at low E_{col}, we have used the RRKM program to calculate the lifetime of precursor 2 ($[Trp\text{-}H]^-$) and H4 as a function of E_{col}. All decomposition channels of precursor 2 ($[Trp\text{-}H]^-$) and H4 indicated by dashed lines in Figure 7b were included. No barrier is expected for decay of the precursor complex back to the reactants (i.e., no reaction) in excess of the asymptote, thus an orbiting transition state[96] was assumed. Rotation quantum number K was treated as active in evaluating unimolecular rate constant k (E, J), so that all ($2J$ + 1) K levels were counted,[97] i.e.

$$k(E, J) = \frac{d}{h}\frac{\sum_{K=-J}^{J} G(E - E_0 - E_r^+(J, K))}{\sum_{K=-J}^{J} N(E - E_r(J, K))}$$

where d is the reaction path degeneracy, G is the transition state sum of states, N is the reactant density of states, E_0 is the unimolecular dissociation threshold, and E_r and $E_r^\dagger$ are the rotational energy for the reactant and the transition state, respectively. The orbital angular momentum L of the precursor complex was estimated from the collision cross section, i.e., $L = \mu v_{rel}(\sigma_{collision}/\pi)^{1/2}$, where μ and v_{rel} are the reduced mass and relative velocity of collision partners, respectively. The orbital angular momentum of H4 was estimated similarly, except that in this case we used $\sigma_{reaction}$ instead of $\sigma_{collision}$ since most of the collisions producing H4 would ultimately lead to products. Complexes and TSs were described using scaled frequencies, polarizabilities, and momentums of inertia from DFT calculations.

As we discussed above, the mechanistic importance of a precursor complex depends on its lifetime. If long enough lived, a precursor complex can allow repeated encounters between two reactants, increasing the probability of eventually finding a low energy pathway to H4. Analogous complexes play an important role in the reactions of $TyrH^+$ + $^1O_2$[43] and $TrpH^+$ + $^1O_2$,[39] for example. At E_{col} lower than 0.2 eV, the lifetime of precursor 2 ($[Trp\text{-}H]^-$) varies from 1 to 50 ns, much longer than the classical rotational period of this complex which is 8–13 ps, and the "fly by" time (as defined above) which ranges from 1.2 ps at E_{col} = 0.1 eV to 0.54 ps at E_{col} = 0.5 eV. We note that the precursor lifetime decreases quickly with increasing E_{col}, dropping to less than 30 ps at E_{col} = 0.5 eV. The lifetime of H4 is longer than that of precursor 2, presumably because of H4 being trapped between two tight transition states. Therefore, these complex lifetimes are in the right range and have the right E_{col} dependence. The conclusion is that these complexes, if form efficiently, could conceivably have mechanistic significance at least for low energies, and the formation of H4 is expected to be the rate-limiting step.

The existence of suitable complexes does not mean that the mechanism is necessarily complex-mediated. A better test is to compare the experimental and RRKM predicted reaction efficiency. RRKM calculations predict that the dominant decay channel for precursor 2 ($[Trp\text{-}H]^-$) corresponds to decaying back to reactants. One related issue in decay of the precursor complex back to reactants is physical quenching of

dx.doi.org/10.1021/jp303022b | J. Phys. Chem. B 2012, 116, 6369–6379

$^1O_2$. It is well established that Trp is capable of significantly quenching $^1O_2$ physically. Such quenching could occur via electronic to vibrational energy transfer between separating reactants in the precursor complex.[15] The net branching ratio for interconversion of precursor 2 to H4 is ~1% at E_{col} = 0.05 eV, decreasing to 0.12% at E_{col} = 0.1 eV and <0.1% at E_{col} = 0.5 eV. For comparison, the experimental reaction efficiencies are 1.1%, 0.9%, and 0.4% at E_{col} = 0.05, 0.1, and 0.5 eV, respectively. Assuming H4 predominantly decays to products, a complex-mediated model is able to reproduce the decrease of the reaction cross section when increasing E_{col}. This suggests that complex mediation may be important at the lowest energies. However, RRKM predicates a much faster decrease of the cross section with increasing E_{col} than was observed experimentally. For example, at E_{col} = 0.5 eV, the experimental reaction efficiency is about four times larger than the RRKM predicted value, suggesting that complex mediation is a minor mechanism for energies above a few tenths of an electronvolt.

IV. CONCLUSIONS

We have employed guided-ion-beam mass spectrometry to determine the reaction products, cross sections, and collision energy dependence for the reactions of $[Tyr-H]^-$ and $[Trp-H]^-$ with $O_2[a^1\Delta g]$. $[Tyr-H]^-$ and $[Trp-H]^-$ have a carboxylate anion structure in the gas phase, and a similar reaction path was observed for these two reactions. Both reactions lead to elimination of H_2O_2 and CO_2 from reaction intermediates, yielding product ions of 4-(2-aminovinyl)-phenolate for $[Tyr-H]^-$ and 3-(2-amionvinyl)indol-1-ide for $[Trp-H]^-$, respectively. However, the reaction of $[Tyr-H]^-$ bears an activation barrier above the reactants, while that of $[Trp-H]^-$ is barrierless. Density functional theory calculations were employed to propose reaction paths leading to the observed product ions, and RRKM theory was used to verify the significance of these reaction paths and predict the collision energy dependence of reaction efficiency. Quasi-classical, direct dynamics trajectories were simulated for $[Tyr-H]^-$ with $^1O_2$ at a collision energy of 0.75 eV using B3LYP/4-31* method. Trajectory results confirm the importance of a complex-mediated mechanism. The combination of experimental and theoretical approaches allows us to ascertain the reaction mechanisms involved in oxidation of $[Tyr-H]^-$ and $[Trp-H]^-$, as well as the effects of deprotonation vs. protonation on reactions.

One interesting result we reported in the gas-phase reactions of protonated $TyrH^{+}$[43] and $MetH^{+}$[49] with $^1O_2$ is that short-lived $^1O_2$ could produce stable H_2O_2 during amino acid oxidation. The present work exemplifies other two systems where H_2O_2 is produced from the reactions of deprotonated amino acids with $^1O_2$. H_2O_2 can diffuse to distant targets in biological systems and thereby initiate damage at sites remote from its initial generation site, and the subsequent reaction of H_2O_2 may play a role in bystander damage or dark-reactions in photosensitization.[37]

AUTHOR INFORMATION

Corresponding Author

*E-mail: jianbo.liu@qc.cuny.edu.

Notes

The authors declare no competing financial interest.

ACKNOWLEDGMENTS

This work was supported by the National Science Foundation CAREER Award (No. CHE-0954507), Queens College Research Enhancement Funds, and PSC-CUNY Research Awards. F.L. and Y.F. are the recipients of the CUNY Doctoral Students Research Grant in 2012.

REFERENCES

(1) Schweitzer, C.; Schmidt, R. *Chem. Rev.* **2003**, *103*, 1685−1757.
(2) Frimer, A. A. *Singlet Oxygen, Vol I, Physical-Chemical Aspects.*; CRC Press: Boca Raton, FL, 1985.
(3) Frimer, A. A. *Singlet Oxygen, Vol II, Reaction Modes and Products, Part 1*; CRC Press: Boca Raton, FL, 1985.
(4) Frimer, A. A. *Singlet O_2, Vol III, Reaction Modes and Products, Part 2*; CRC Press: Boca Raton, FL, 1985.
(5) Frimer, A. A. *Singlet O_2, Vol IV, Polymers and Biomolecules*; CRC Press: Boca Raton, FL, 1985.
(6) Sawyer, D. T. *Oxygen Chemistry*; Oxford University Press: New York, 1991.
(7) Ogilby, P. R. *Chem. Soc. Rev.* **2010**, *39*, 3181−3209.
(8) Davies, M. J. *Biochem. Biophys. Res. Commun.* **2003**, *305*, 761−770.
(9) Morgan, P. E.; Dean, R. T.; Davies, M. J. *Free Radical Biol. Med.* **2004**, *36*, 484−496.
(10) Davies, M. J. *Biochim. Biophys. Acta* **2005**, *1703*, 93−109.
(11) Palumbo, G. *Expert Opin. Drug Delivery* **2007**, *4*, 131−148.
(12) Baker, A.; Kanofsky, J. R. *Photochem. Photobiol.* **1992**, *55*, 523−528.
(13) Davies, M. J. *Photochem. Photobiol. Sci.* **2004**, *3*, 17−25.
(14) Foote, C. S. *Science* **1968**, *162*, 963−970.
(15) Wilkinson, F.; Helman, W. P.; Ross, A. B. *J. Phys. Chem. Ref. Data* **1995**, *24*, 663−667.
(16) Wright, A.; Hawkins, C. L.; Davis, M. J. *Redox Report* **2000**, *5*, 159−161.
(17) Wright, A.; Bubb, W. A.; Hawkins, C. L.; Davies, M. J. *Photochem. Photobiol.* **2002**, *76*, 35−46.
(18) Weil, L.; Gordon, W. G.; Buchert, A. R. *Arch. Biochem.* **1951**, *33*, 90−109.
(19) Sluyterman, L. A. *Biochem. Biophys. Acta* **1962**, *60*, 557−561.
(20) Weil, L. *Arch. Biochem. Biophys.* **1965**, *110*, 57−68.
(21) Bellin, J. S.; Yankus, C. A. *Arch. Biochem. Biophys.* **1968**, *123*, 18−28.
(22) Spikes, J. D.; MacKnight, M. L. *Ann. N.Y. Acad. Sci.* **1970**, *171*, 149−162.
(23) Fishman, P. H.; Kusiak, J. W.; Bailey, J. M. *Biochem.* **1973**, *12*, 2540−2544.
(24) Rizzuto, F.; Spikes, J. D. *Photochem. Photobiol.* **1977**, *25*, 465−476.
(25) Papeschi, G.; Monici, M.; Pinzauti, S. *Med. Biol. Environ.* **1982**, *10*, 245−250.
(26) Bertolotti, S. G.; Garcia, N. A.; Arguello, G. A. *J. Photochem. Photobiol. B: Biol.* **1991**, *10*, 57−70.
(27) Criado, S.; Soltermann, A. T.; Garcia, N. A. *Amino Acids* **1995**, *8*, 367−377.
(28) Criado, S.; Marioli, J. M.; Allegretti, P. E.; Furlong, J.; Nieto, F. J. R.; Martire, D. O.; Garcia, N. A. *J. Photochem. Photobiol. B: Biol.* **2001**, *65*, 74−84.
(29) Bisby, R. H.; Morgan, C. G.; Hamblett, I.; Gorman, A. A. *J. Phys. Chem. A* **1999**, *103*, 7454−7459.
(30) Posadaz, A.; Biasutti, A.; Casale, C.; Sanz, J.; Amat-Guerri, F.; Garcia, N. A. *Photochem. Photobiol.* **2004**, *80*, 132−138.
(31) Matheson, I. B. C.; He, J. *Photochem. Photobiol.* **1979**, *29*, 879−881.
(32) Vollhardt, P.; Schore, N. *Organic Chemistry*, 6th ed.; W. H. Freeman and Company: New York, 2009.
(33) Jolley, M. E.; Gxay, C. J. *Carbohydr. Res.* **1976**, *49*, 361−370.

(34) Nakagawa, M.; Watanabe, H.; Kodato, S.; Okajima, H.; Hino, T.; Flippen, J. L.; Witkop, B. *Proc. Natl. Acad. Sci. U.S.A.* **1977**, *74*, 4730−4733.
(35) Saito, I.; Matsuura, T.; Nakagawa, M.; Hino, T. *Acc. Chem. Res.* **1977**, *10*, 346−352.
(36) Langlots, R.; H. Ali, N. B.; Wagner, J. R.; Lier, J. E. v. *Photochem. Photobiol.* **1986**, *44*, 117−123.
(37) Gracanin, M.; Hawkins, C. L.; Pattison, D. I.; Davies, M. J. *Free Radical Biol. Med.* **2009**, *47*, 92−102.
(38) Grosvenor, A. J.; Morton, J. D.; Dyer, J. M. *Amino Acids* **2010**, *39*, 285−296.
(39) Liu, F.; Fang, Y.; Chen, Y.; Liu, J. *J. Phys. Chem. B* **2011**, *115*, 9898−9909.
(40) Palumbo, M. C.; Garcia, N. A.; Arguello, G. A. *J. Photochem. Photobiol. B: Biol.* **1990**, *7*, 33−42.
(41) Yagil, G. *Tetrahedron* **1969**, *23*, 2855−2861.
(42) Sysak, P. K.; Foote, C. S.; Ching, T.-Y. *Photochem. Photobiol.* **1977**, *26*, 19−27.
(43) Fang, Y.; Liu, J. *J. Phys. Chem. A* **2009**, *113*, 11250−11261.
(44) Yamashita, M.; Fenn, J. B. *J. Phys. Chem.* **1984**, *88*, 4451−4459.
(45) Fenn, J. B.; Mann, M.; Meng, C. K.; Wong, S. F.; Whitehouse, C. M. *Science* **1989**, *246*, 64−71.
(46) Gerlich, D. Inhomogeneous RF fields: A versatile tool for the study of processes with slow ions. In *State-Selected and State-to-State Ion−Molecule Reaction Dynamics. Part I. Experiment*; Ng, C. Y., Baer, M., Eds.; John Wiley & Sons, Inc.: New York, 1992; Vol. *82*, pp 1−176.
(47) Marcus, R. A. *J. Chem. Phys.* **1952**, *20*, 359−364.
(48) Hase, W. L.; Song, K.; Gordon, M. S. *Comput. Sci. Eng.* **2003**, *5*, 36−44.
(49) Fang, Y.; Liu, F.; Bennett, A.; Ara, S.; Liu, J. *J. Phys. Chem. B* **2011**, *115*, 2671−2682.
(50) Fehsenfeld, F. C.; Albritton, D. L.; Burt, J. A.; Schiff, H. I. *Can. J. Chem.* **1969**, *47*, 1793−1795.
(51) Schmitt, R. J.; Bierbaum, V. M.; DePuy, C. H. *J. Am. Chem. Soc.* **1979**, *101*, 6443−6445.
(52) Bierbaum, V. M.; Schmitt, R. J.; DePuy, C. H. *Environ. Heath Perspect.* **1980**, *36*, 119−124.
(53) Grabowski, J. J.; Van Doren, J. M.; DePuy, C. H.; Bierbaum, V. M. *J. Chem. Phys* **1984**, *80*, 575−577.
(54) Dotan, I.; Barlow, S. E.; Ferguson, E. E. *Chem. Phys. Lett.* **1985**, *121*, 38−40.
(55) Upschulte, B. L.; Marinelli, W. J.; Green, B. D. *J. Phys. Chem.* **1994**, *98*, 837−842.
(56) Midey, A.; Dotan, I.; Lee, S.; Rawlins, W. T.; Johnson, M. A.; Viggiano, A. A. *J. Phys. Chem. A* **2007**, *11*, 5218−5222.
(57) Midey, A.; Dotan, I.; Viggiano, A. A. *J. Phys. Chem. A* **2008**, *112*, 3040−3045.
(58) Midey, A. J.; Dotan, I.; Viggiano, A. A. *Int. J. Mass Spectrom.* **2008**, *273*, 7−10.
(59) Midey, A.; Dotan, I.; Seeley, J. V.; Viggiano, A. A. *Int. J. Mass Spectrom.* **2009**, *280*, 6−11.
(60) Viggiano, A. A.; Midey, A.; Eyet, N.; Bierbaum, V. M.; Troe, J. *J. Chem. Phys.* **2009**, *131*, 094303/094301−0943930/0943936.
(61) Eyet, N.; Midey, A.; Bierbaum, V. M.; Viggiano, A. A. *J. Phys. Chem. A* **2010**, *114*, 1270−1276.
(62) Eyet, N.; Viggiano, A. A. *J. Phys. Chem. A* **2010**, *114*, 7506−7508.
(63) Fang, Y.; Bennett, A.; Liu, J. *Int. J. Mass Spectrom.* **2010**, *293*, 12−22.
(64) Fang, Y.; Bennett, A.; Liu, J. *Phys. Chem. Chem. Phys.* **2011**, *13*, 1466−1478.
(65) Moision, R. M.; Armentrout, P. B. *J. Am. Soc. Mass Spectrom.* **2007**, *18*, 1124−1134.
(66) Krutchinsky, A. N.; Chernushevich, I. V.; Spicer, V. L.; Ens, W.; Standing, K. G. *J. Am. Soc. Mass Spectrom.* **1998**, *9*, 569−579.
(67) Douglas, D. J.; French, J. B. *J. Am. Mass Spectrom.* **1992**, *3*, 398−408.
(68) Ervin, K. M.; Armentrout, P. B. *J. Chem. Phys.* **1985**, *83*, 166−189.
(69) Armentrout, P. B. *J. Anal. At. Spectrom.* **2004**, *19*, 571−580.
(70) Seliger, H. H. *Anal. Biochem.* **1960**, *1*, 60−65.
(71) Khan, A.; Kasha, M. *J. Chem. Phys.* **1963**, *39*, 2105−2106.
(72) Lafferty, W. J.; Solodov, A. M.; Lugez, C. L.; Fraser, G. T. *Appl. Opt.* **1998**, *37*, 2264−2270.
(73) Troe, J. *Chem. Phys. Lett.* **1985**, *122*, 425−430.
(74) Frisch, M. J.; Trucks, G. W.; Schlegel, H. B.; Scuseria, G. E.; Robb, M. A.; Cheeseman, J. R.; Scalmani, G.; Barone, V.; Mennucci, B.; Petersson, G. A.; et al. *Gaussian 09*, revision B. 01; Gaussian, Inc.: Wallingford, CT, 2009.
(75) Matxain, J. M.; Ristilae, M.; Strid, A.; Eriksson, L. A. *Chem.—Eur. J.* **2007**, *13*, 4636−4642.
(76) Zheng, J.; Alecu, I. M.; Lynch, B. J.; Zhao, Y.; Truhlar, D. G. Database of Frequency Scale Factors for Electronic Model Chemistries, Version 2; http://comp.chem.umn.edu/freqscale/version2.htm, 2010.
(77) Zhu, L.; Hase, W. L. A General RRKM Program(QCPE 644), Quantum Chemistry Program Exchange; Chemistry Department, University of Indiana: Bloomington, 1993.
(78) Hase, W. L.; Bolton, K.; de Sainte Claire, P.; Duchovic, R. J.; Hu, X.; Komornicki, A.; Li, G.; Lim, K.; Lu, D.; Peslherbe, G. H.; et al.. VENUS99: A general chemical dynamics computer program; Texas Tech Univeristy: Lubbock, TX, 1999.
(79) Bakken, V.; Millam, J. M.; Schlegel, H. B. *J. Chem. Phys.* **1999**, *111*, 8773−8777.
(80) Bacskay, G. B. *Chem. Phys.* **1981**, *61*, 385−404.
(81) Laaksonen, L. gOpenMol; 3.0 ed.; Center for Scientific Computing: Espoo, Finland, 2005; available at www.csc.fi/gopenmol/.
(82) Liu, J.; Song, K.; Hase, W. L.; Anderson, S. L. *J. Chem. Phys.* **2003**, *119*, 3040−3050.
(83) Liu, J.; Song, K.; Hase, W. L.; Anderson, S. L. *J. Phys. Chem. A* **2005**, *109*, 11376−11384.
(84) Levine, R. D.; Bernstein, R. B. *Molecular Reaction Dynamics and Chemical Reactivity*; Oxford University Press: New York, 1987.
(85) Liu, J.; Anderson, S. L. *J. Chem. Phys.* **2004**, *120*, 8528−8536.
(86) Kulik, W.; Heerma, W. *Biomed. Environ. Mass Spectrom.* **1988**, *15*, 419−427.
(87) Waugh, R. J.; Bowie, J. H.; Hayes, R. N. *Int. J. Mass Spectrom. Ion Processes* **1991**, *107*, 333−347.
(88) Couldwell, A. M.; Thomas, M. C.; Mitchell, T. W.; Hulbert, A. J.; Blanksby, S. J. *Rapid Commun. Mass Spectrom.* **2005**, *19*, 2295−2304.
(89) Tian, Z.; Wang, X.-B.; Wang, L.-S.; Kass, S. R. *J. Am. Chem. Soc.* **2009**, *131*, 1174−1181.
(90) Ervin, K. M.; Lineberger, W. C. *J. Phys. Chem. A* **2003**, *107*, 8521−8529.
(91) Jones, C. M.; Bernier, M.; Carson, E.; Colyer, K. E.; Metz, R.; Pawlow, A.; Wischow, E. D.; Webb, I.; Andriole, E. J.; Poutsma, J. C. *Int. J. Mass Spectrom.* **2007**, *267*, 54−62.
(92) Tian, Z.; Kass, S. R. *J. Am. Chem. Soc.* **2008**, *130*, 10842−10843.
(93) Oomens, J.; Steill, J. D.; Redlich, B. *J. Am. Chem. Soc.* **2009**, *131*, 4310−4319.
(94) Bradford, A. M.; Waugh, R. J.; Bowie, J. H. *Rapid Commun. Mass Spectrom.* **1995**, *9*, 677−685.
(95) Compagnon, I.; Allouche, A.-R.; Bertorelle, F.; Antoine, R.; Dugourd, P. *Phys. Chem. Chem. Phys.* **2010**, *12*, 3399−3403.
(96) Rodgers, M. T.; Ervin, K. M.; Armentrout, P. B. *J. Chem. Phys.* **1997**, *106*, 4499−4508.
(97) Zhu, L.; Hase, W. L. *Chem. Phys. Lett.* **1990**, *175*, 117−124.